Track MS status:
May 4th 2025 – First version submitted to EarthArXiv and Earth Science Reviews (Elsevier)
May 7th 2025 – Editorial rejection (out of scope for a large review journal)
May 9th, 2025 – Submitted to Quaternary Science Reviews (Elsevier)
September 12th, 2025 – Rejected after reviews, possible resubmission indicated by editor

The Apalachicola Barrier Island complex: a benchmark for MIS 5e (125 ka) sea-level oscillations?

Nikos Georgiou[1], Alexander R. Simms[2], Roger C. Creel[3], Silas Dean[1], Denovan Chauveau[4], Ciro Cerrone[1], Claudia Caporizzo[5], Alessio Rovere[1,6]

[1] University of Venice Ca' Foscari, Department of Environmental Sciences, Informatics and Statistics, Scientific Campus Via Torino 155, 30172 Mestre (VE), Italy
[2] Department of Earth Science, University of California Santa Barbara, Santa Barbara, CA 93106, USA
[3] Woods Hole Oceanographic Institution, Woods Hole, Massachusetts 02543-1050, USA
[4] Geo-Ocean, UMR 6538, CNRS, Ifremer, Université de Bretagne Occidentale, F-29280 Plouzané, France
[5] Università Telematica Pegaso, Centro Direzionale Isola F2, 80143, Napoli, Italy
[6] MARUM, Center for Marine Environmental Sciences, University of Bremen, Leobener Str. 8, 28359 Bremen, Germany

Correspondence to: Alessio Rovere (alessio.rovere@unive.it)

Abstract

Coastal sandy barrier systems develop under moderate wave energy, sufficient sediment supply, and adequate accommodation space, and can preserve critical paleoenvironmental records of past sea-level variations, climatic shifts, and storm histories within their geomorphological and stratigraphic frameworks. Beach ridges, identifiable on both horizontal (ridge-swale morphology) and vertical (internal sedimentary structures) planes, record wave regime shifts, storm impacts, and sea-level changes. Recent methodological advances such as Ground Penetrating Radar (GPR), LiDAR topography, and Optically Stimulated Luminescence (OSL) dating now allow for high-resolution reconstructions of these past coastal dynamics, significantly improving our understanding of historical shoreline evolution. We first review how these systems have been used to reconstruct past climate conditions and coastal processes, then apply these concepts to investigate the evolution of the Apalachicola Barrier Island Complex in northwest Florida during the Last Interglacial (MIS 5e, ~125 ka). By integrating new GPR surveys with existing LiDAR data and OSL chronologies, we found that the Apalachicola complex was formed in two distinct phases linked to early and late MIS 5e sea-level highstands, separated by an erosional unconformity marking a rapid mid-MIS 5e regression and fluvial incision. Renewed transgression in late MIS 5e led to seaward barrier progradation, forming younger beach ridges. GPR profiles record multiple buried storm scarps, indicating major storms approximately every 75–80 years. Paleogeographic reconstructions show significant barrier morphological changes, including island segmentation and deltaic interactions, driven by sea-level fluctuations. Our findings offer a missing piece of evidence that helps refine reconstructions of MIS 5e sea-level variability.

1. Introduction

Sedimentary coastal systems respond to different forcings by prograding (i.e., advancing horizontally), retreating and accreting (growing vertically) as a response to changes in sea level (Okazaki et al., 2022), storm intensity and direction (Buynevich et al., 2007; Goodwin et al., 2023), sediment supply, and shoreline evolution (Dougherty, 2018). Prograding sand barriers serve as near-continuous records of paleoenvironmental signals, and studies on their evolution have advanced in the last decades thanks to the development of techniques such as Light Detection and Ranging (LiDAR), Ground Penetrating Radar (GPR), and Optically Stimulated Luminescence (OSL) dating (Fairbridge and Hillaire-Marcel, 1977; Gernant et al., 2025; Rodriguez and Meyer, 2006; Scheffers et al., 2012). These methods allow high-resolution studies of surface and subsurface morphological features, and establishing chronological sequences, detailing the evolution of sand barriers.

Prograded sandy coastal barriers are depositional landforms found globally in a range of geological, climatic, and sea-level contexts (Otvos, 2000). They can develop during both transgressive and regressive sea levels (Boyd et al., 1992). Typically, they form in shallow and flat coastal areas with sufficient accommodation and substantial sediment supply, which can be sourced from either fluvial or long/cross-shore transport (Scheffers et al., 2012). Moderate wave energy is also a key factor in the formation and maintenance of a sandy coastal barrier. Wave energy needs to be strong enough to move sediment above the mean spring tide level, but not so strong that erosion exceeds deposition. Beyond sediment discharge, wind, storms, and tidal ranges also govern coastal barrier morphology (Isla et al., 2023; Tamura, 2012). When sediment accumulation exceeds available accommodation, coastal barriers advance seaward, forming systems that preserve near-continuous paleoclimatic and morphodynamic geo-archives (Hein and Ashton, 2020). Under regressive conditions, these systems manifest as sequences of beach ridges and spits, while barrier islands and estuarine strandplains form under transgressive environments (Isla et al., 2023).

While studies on Holocene coastal barriers are widespread, fewer studies address Pleistocene coastal barriers, which are generally found landward of their Holocene counterparts. In this paper, we first review how prograding sandy coastal barriers have been used to reconstruct past climate conditions and coastal processes, including variations in sea level, sediment transport, wave energy, and storm activity. We then apply these concepts to interpret the evolution of the Apalachicola composite barrier system in Florida, USA. At this location, we merge new ground-penetrating radar (GPR) data from beach ridges with high-resolution Digital Elevation Models (DEMs) and a reanalysis of existing optically stimulated luminescence (OSL) ages. We use these resources to shed light on sea-level oscillations and storm frequency that characterized the Last Interglacial (Marine Isotopic Stage, MIS , 5e, 125 ka) history of the Apalachicola beach barrier complex.

2. Coastal barriers as paleoclimate proxies

Among prograding sandy barriers, beach ridge systems stand out as particularly valuable archives of paleo-environmental information, which can be extrapolated by landforms identifiable on either the horizontal or vertical plane. These are briefly described below, with reference to those more closely related to sea level at the time of their formation.

2.1 Horizontal Plane Beach Ridge Geometry

Beach ridge systems are composed of prograding ridges and swales that run parallel or semi-parallel to shore (Taylor and Stone, 1996). Their relief is usually attributed to a foredune ridge that develops when vegetation on the back barrier traps aeolian sand. However, lower relief ridges may form without an aeolian cap, and the back barrier's role in shaping this relief remains debated (Hesp, 1984). In a single system, some ridge-swale pairs can take a century to form; other pairs can form in a single storm event. Beach ridge sediment deposition is influenced by factors such as shoreline progradation rate, sediment supply, fluvial discharge, wave conditions, and erosion events (Tamura, 2012); ridge spacing varies between 30-90 m and depends on the sediment supply (Isla et al., 2023). As a shoreline progrades, older ridge sets deactivate and become isolated. Relict shoreline asymmetry in orientation and/or geometry is indicative of shifts in the dominant wave direction, fluvial discharge and/or sediment supply, and beach morphodynamic response (Goodwin et al., 2020; Lindhorst and Schutter, 2014; Nienhuis et al., 2016). These indicators can be observed in fossilized ridge systems that formed during the Holocene and Pleistocene, allowing the comparison of environmental processes across different periods. Schematic representations of the effect of various processes on beach ridge strandplain geometry are shown in Figure 1.

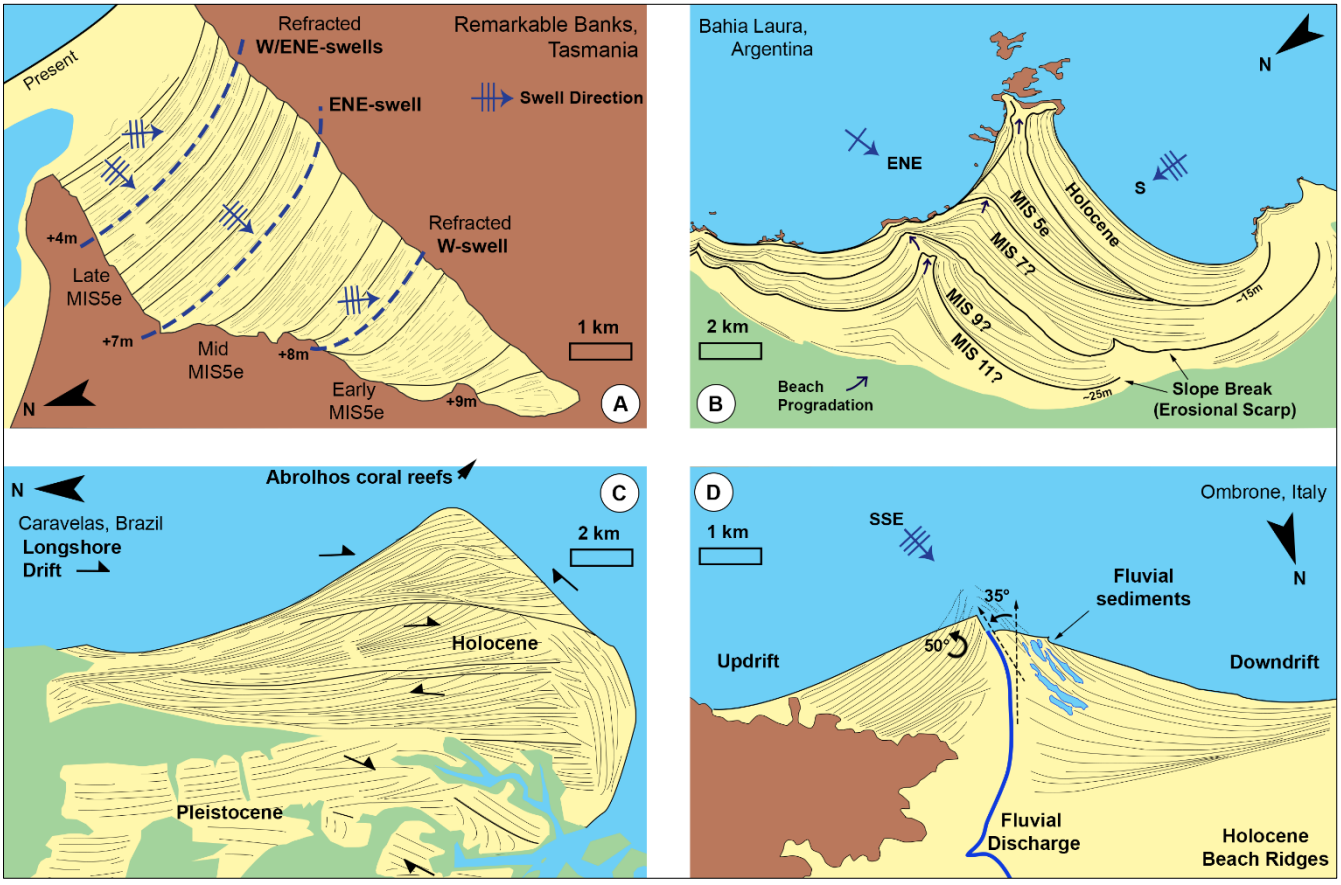

Figure 1. Schematic interpretation of beach ridge strandplains on the horizontal plane showing the effect of different processes on the strandplains' geometry: A) Wave-regime shifting (modified after Goodwin et al., 2023). B) uplift and coastal geomorphology (modified after Pedoja et al., 2011- black arrows indicate the influence of rocky outcrops to the evolution of the strandplain). C) longshore drift shift and costal geomorphology (modified after Andrade et al., 2003). D) sediment flux and anthropogenic influence (modified after Mammì et al., 2019; Nienhuis et al., 2016; Pranzini, 2024).

Changes in the orientation of a beach ridge strandplain allowed Goodwin et al., (2023, Figure 1A) to reconstruct the MIS5e paleo wave climate history, which deviates from the modern wave regime in Tasmania. Through LiDAR elevation data, numerical modelling, and morphometric analysis, three direction-shifting wave phases were revealed: Phase 1 saw the dominance of Southern Ocean W/SW swells, Phase 2 experienced a shift to low-energy NE-E wave climate, and Phase 3 returned to a bimodal wave direction characterized by W/SW and E-NE swells. A 5° poleward shift of the Subtropical Ridge and a general tropical expansion was also revealed when the current and paleo-shoreline geometry were compared (Figure 1A). The strandplain's elevation was found to be mainly controlled by relative sea-level (RSL) changes with a notable stillstand in RSL during Phase 2, at 5.75 ± 0.5 m above modern sea level, providing insights into the GIA-induced (Glacial Isostatic Adjustment) regression, which was equalized by the persistent meltwater contributions (Goodwin et al., 2023).

Composite Pleistocene-Holocene beach ridge systems formed in Bahía Laura, Argentina (Figure 1B) exhibit the effect of vertical land motions caused by a combination of GIA and dynamic topography (e.g. Rubio-Sandoval et al., 2024), with a sequence of at least five marine terraces including beach ridge sequences that date back to MIS11 (Pedoja et al., 2011). The planform geometry indicates the influence of coastal geomorphology on beach progradation, as each sequence forms a tombolo connecting to the nearest rocky formation (black arrows, Figure 1B).

Longshore drift direction can be imprinted on beach ridges orientation as found in the composite Caravelas strandplain, Brazil (Figure 1C), whose formation is largely controlled by the interaction between RSL changes and the development of the Abrolhos coral reefs (Andrade et al., 2003). The truncations and alignments of the beach ridges serve as indicators of shifts in sediment transport along the coast. These truncations likely occur when changes in longshore drift interrupt ridge formation; longshore drift was in turn likely influenced by changes in offshore coral reef growth further east, which altered sediment accumulation and switched longshore sediment transport direction. This suggests that reef growth and degradation had a significant impact on sediment dispersal and beach ridge formation.

In the Ombrone delta, Italy, deforestation over the last 2.5 kyr increased fluvial sediment supply, resulting in beach ridge updrift rotating by 50° and channels reorienting (35° updrift) towards incoming waves (Nienhuis et al., 2016; Pranzini, 2024) (Figure 1D). This morphological shift suggests that river channels tend to align with incoming waves when the fluvial sediment flux is high. Part of the prograded coast later eroded when reforestation, damming, and quarrying decreased sediment flux (Figure 1D, seaward dashed lines, Mammì et al., 2019).

2.2 Vertical Plane Beach Ridge Geometry

The internal vertical architecture of beach ridges can be studied using ground penetrating radar (GPR) surveys. Prograding beach ridges form seaward-inclined deposits whose inclination can reach up to 6° (fine-coarse sand) (Tamura, 2012) and is steeper for coarser grains (Jol et al., 1996) and lower wave energy (Hede et al., 2013; Phillips et al., 2019). These inclined beds appear as clinoforms on GPR profiles (Figure 2A) with those that show a higher intensity indicating truncation surfaces caused by reduced sediment supply, coarse grained sediment, or high-energy events (Buynevich et al., 2007). Landward dipping deposits are less common but occur when washover or bar deposits form (Taylor and Stone, 1996; Zurbuchen et al., 2020). Progradation rates may vary from few centimetres to 30 meters annually depending on sediment flux and accommodation (Hein and Ashton, 2020). Upwards, the beachface most frequently abuts aeolian sediment, with flat lying reflectors marking the transition to dune ridges and the beach-dune (BD) contact (Tamura, 2012).

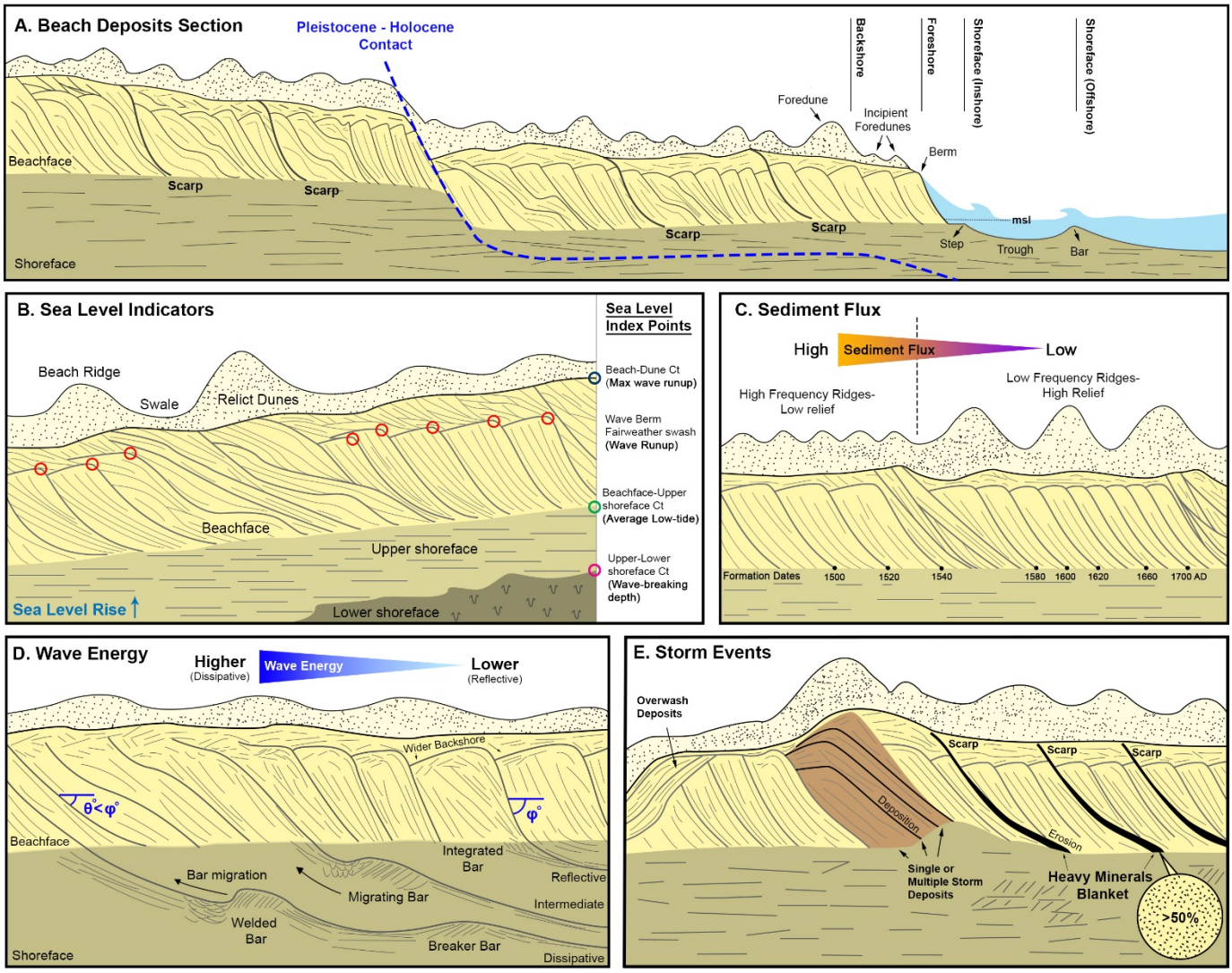

Figure 2. Idealized stratigraphic profiles showing common vertical plane geometries and the impact of varying climatic forcings on foreshore and shoreface deposits. A) Composite Holocene-Pleistocene beach deposit section, after Dougherty, 2018. MSL is mean sea level. B) Sea level rise, after Costas et al., 2016. Ct is contact. C) Sediment flux. D) Wave energy. E) Storm events.

Foredune ridge development depends on factors such as waves, wind, tides, sediment budget, sea-level history and vegetation density (Ciarletta et al., 2019) and is expressed as landward, seaward, or cross-bedded reflections on the GPR profiles. The upper shoreface, underlying the beachface, is usually recognised by high-angle trough crossbedding aligned parallel to the shoreline with crossbedding rarely preserved while laminated or structureless sand can be found in the lower shoreface (Clifton, 2005).

Beach ridges are regularly used to reconstruct past sea levels (Gernant et al., 2025; Kumar et al., 2024; Mauz et al., 2013; Montes et al., 2018; Stattegger et al., 2013). These features are often considered Sea Level Index Points (SLIPs), which are points that delimit both an age and elevation range rather than merely an upper or lower limit to past sea level (Shennan, 1986; Shennan et al., 2015). The foreshore facies most commonly used to reconstruct SLIPs are the Beach - Dune contact, wave berm, Beachface - Upper shoreface contact, and Upper - Lower shoreface contact (Costas et al., 2016; Tamura et al., 2007, Figure 2B). The Beach - Dune contact, the uppermost stratigraphically identified SLIP, marks the maximum runup of storm waves and is recognised by strong, wavy, sub-horizontal, subparallel reflections, with the dipping beachface below showing truncation or toplap structures (Costas et al., 2016). The wave berm, characterized by a slope change at the seaward margin and a flat or landward sloping platform, marks the upper limit of the fairweather swash zone (Costas et al., 2016; Otvos, 2000). Seaward-dipping reflections forming downlap points on the upper shoreface indicate average low-tide sea levels and are considered reliable SLIPs as they capture both high and low sea levels and are the last to erode from the foreshore facies (Hede et al., 2013; Nielsen et al., 2017). The erosional contact between the upper and lower shoreface, created by longshore trough migration, can also be a SLIP, though its precision depends on local wave-breaking depth (Hede et al., 2013).

Variations in the sediment flux, whether of anthropogenic or climatic origin, directly affect the beach ridge frequency and spacing over timescales ranging from months to millennia (Figure 2C, Hein and Ashton, 2020; Tamura, 2012). Sediment-starved areas tend to form foredune ridges of higher relief and wider spacing than quickly prograding beaches (Carvalho et al., 2019; Nooren et al., 2017; Ruz and Allard, 1994), since sediment starvation leaves dunes more time to accumulate aeolian sand prior to being blocked by a newer dune created by the prograding beach face with its newer sediments. The inverse pattern applies for quickly prograding beach units: higher spatial frequency and lower temporal frequency occurring under conditions of high sediment flux.

Minor variations in wave energy, not including destructive or extreme events, can significantly alter the geometry of the beach face as it alternates between dissipative phases that represent high wave energy events and reflective phases deposited under normal wave conditions (Flemming, 1982; Masselink et al., 2006, Figure 2D). Higher wave energy flattens the beach profile and builds offshore bars into the shoreface, which migrate shoreward and become part of the beach as it returns to a reflective profile. Under reflective conditions, the backshore widens, the wave berm expands, and the inclination of the beachface increases.

Storms cause rapid changes along sandy coasts, affecting prograding beach and dune systems, which preserve geological records of these events, both as depositional and erosional landforms (Goslin and Clemmensen, 2017) (Figure 2E). Storms can form build-ups (i.e. high beach ridges), which usually consist of coarse-grained material (coarse sand, shells, gravel) and may be the result of single or multiple storm events. Washover deposits, which contain heavy-minerals, organic content, and shell concentrations, can provide evidence of storm occurrence and intensity (Goslin and Clemmensen, 2017). They can be

recognised by the high energy, landward dipping or horizontal reflectors on GPR profiles of back-barrier sediments, which may form perched fans, sheetwashes, or large scale inlet channels, depending on storm intensity (Carruthers et al., 2013; Donnelly et al., 2006; Masselink and van Heteren, 2014). Even if unconsolidated, large foredunes in prograding beaches prevent storms from breaching barriers, forming erosional scarps by eroding sediments and building bars to the offshore, which are integrated when the beach is restored back to the reflective profile (Buynevich et al., 2007). These erosional storm scarps are preserved in prograding coasts due to the post-storm recovery infill and, when dated, can record paleo-storm frequency and intensity. They are recorded in GPR profiles as high reflectivity, steep seaward dipping strata, and in sediment cores are characterized by heavy minerals (percentage >50%) and coarse-grained material (Dougherty, 2018; Komar and Wang, 1984).

3. The Apalachicola Barrier Island Complex

In this study, we examine a composite coastal barrier located near Apalachicola of the Northeastern Gulf of Mexico. Named the "Apalachicola Barrier Island Complex" (Rink and López, 2010), the complex consists of Pleistocene (MIS5e) beach ridge deposits landward of a Holocene transgressive barrier chain that extends from St Joseph Peninsula to the west to St George barrier island to the east (Burdette et al., 2012, Figure 3). The Apalachicola Barrier Island Complex is one of the most extensive strandplains in the Gulf of Mexico, with almost a 10 km-wide area of discontinuous Pleistocene beach ridges and 6 km of Holocene beach ridges. Supplied by sediment from the Apalachicola River, the Holocene strandplain is welded by the prevailing Southern swells. A northwards prograding spit (St. Joseph Peninsula) and three strandplains prograding towards the south (Cape San Blas, St. Vincent Isl., Little St. George Isl.) constitute the main Holocene coastal barrier system, with the narrow SW-NE extending wave-dominated barrier island of St. George bounding the transgressive Apalachicola Bay to the East (Figure 3B).

The Quaternary coastal surface sediments in the study area (Scott et al., 2001) include several sedimentary units (Figure 3B). Quaternary Holocene Sediments (*Qh*) are mainly marine sands, muds and organics near the present coastline. Quaternary Beach Ridge and Dune (*Qbd*) sediments are composed of beach ridge belts usually consisting of shoreface to foreshore sand; this unit is called the Gulfport formation by Otvos, (1992), a term not implemented in the Florida Geologic Map by Scott et al., 2001. Quaternary Alluvium (*Qal*) of Pleistocene and Holocene age occur mainly in floodplains. And Tertiary/Quaternary Shelly Sediments (*TQSu*) include mainly nearshore fine-grained fossiliferous sediment; this unit was termed the Biloxi formation by Otvos, (1992) but the terminology is not recognized by the Florida Geological Survey (Burdette et al., 2012).

Among the Pleistocene deposits, the age of *Qbd* is controversial: Burdette et al., (2012) cite OSL dates retrieved from coastal sediment cores to suggest that the beach ridges formed during the MIS5e highstand. The formation below the *Qbd* and *Qal* (namely, *TQSu*), showed an OSL saturated signal (Burdette et al., 2012) proposing an older age (MIS7/9) than the MIS 5 age proposed by Otvos, (1992). *Qal* was interpreted as an alluvial cover of MIS6 age overlying the *TQSu*, but Otvos (1992)

highlighted inconsistencies in dating and stratigraphic identification of the *Qal* unit. Deeper sediment cores from the area suggest that the *Qbd* deposits thicken west of the Apalachicola delta, revealing two fining upwards sandy Pleistocene sequences, the younger one dated to ~30 ka and the older attributed to MIS5e (Schnable and Goodell, 1968). The eastern part of the area has been extensively eroded revealing the underlying Miocene-Pliocene formations (Figure 3A).

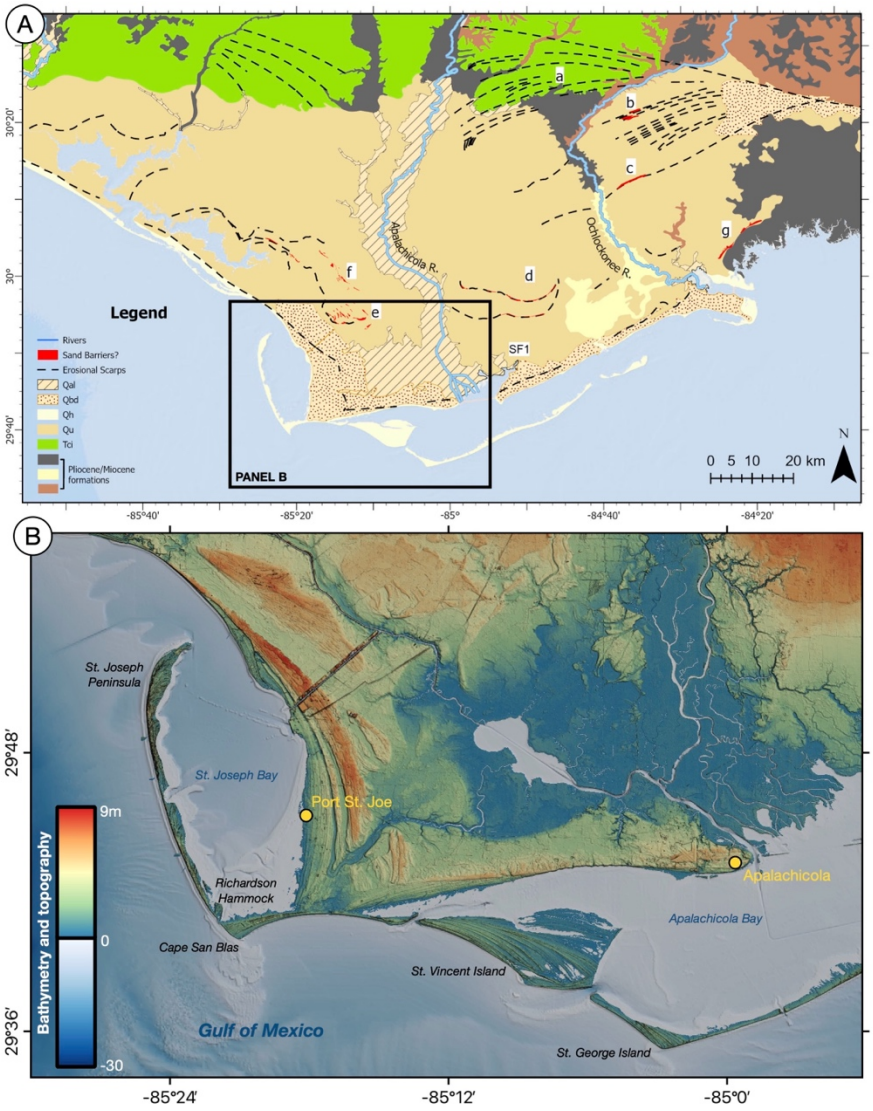

Figure 3. A) Geologic map of the Apalachicola barrier system (from Scott et al., 2001). Red polygons mark sand barriers; dashed black line marks distinct geomorphological features based on the results of former studies. Labels a-g correspond to locations of geomorphological features shown in Figure 4. Label SF1 marks the location of the geomorphological feature represented in Supplementary Figure 1. Legend of geological formations: Qh = Quaternary Holocene Sediments; Qbd = Quaternary Beach Ridge and Dune; Qal = Quaternary Alluvium; Qu = unconsolidated and undifferentiated sediments; Tci = Citronelle Formation. B). Digital elevation model of the study area (NOAA National Centers for Environmental Information, 2023; US Geological Survey, 2011) with toponyms mentioned in the text and main towns.

The existence of Pleistocene terraces and their interpretation as arcuate sand bodies and barrier islands on the unconsolidated and undifferentiated sediments (*Qu* – sand, clay, organics) of the Apalachicola Delta has been contested. Otvos (1995) suggest that these features may be formed by regional tectonic uplift, human activity, e.g. abandoned logging railroad beds and routes or dissolution of underlying carbonates. Conversely, Donoghue et al. (1998) argue for a marine origin of these formations based on sedimentological and geomorphological data (Brenneman and Tanner, 1958; Goetschius, 1971; Stapor Jr et al., 1991), the subsidence of the area (Holdahl and Morrison, 1974), and ionium-disequilibrium dates indicating ages older than MIS5e (Maxwell, 1971a, 1971b).

To better understand the evolution of the Apalachicola delta and test assumptions on the age of the beach ridges imprinted in the landscape, we use the 1/9 arcsecond (~3m) and 1-meter Digital Elevation Models (DEM) from Apalachicola to Pensacola (Figure 3B, US Geological Survey, 2022, 2011) and a detailed geological map (Scott et al., 2001), focusing on linear structures which mark deltaic progradation (dashed black lines in Figure 3A). Starting from the North, the Citronelle Formation (*Tci* in Figure 3A) is the prevailing formation consisting mainly of quartz sand and gravel, partly deposited as river delta deposits in a late Pliocene-Early Pleistocene nearshore environment (Scott et al., 2001). Selective fluvial erosion in a SW-NE orientation, particularly within the Citronelle Formation, formed wedge-shaped channels whose geometry resembles delta progradation deposits of the Apalachicola River formed during the late Pliocene to Early Pleistocene. The SW-NE mounds, possibly related to prograding beach deposits, reach maximum elevation of 40m to 75m (vertical datum: NAVD88, Figure 4A).

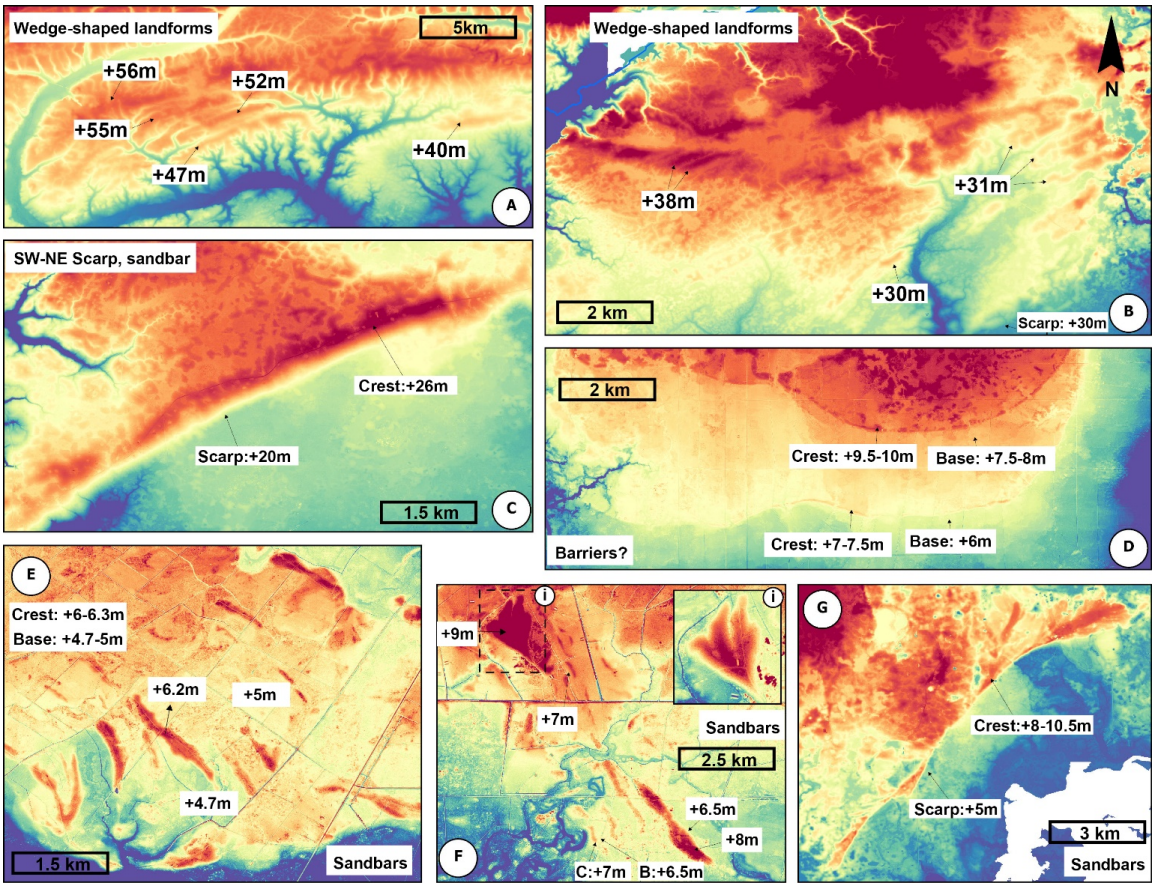

255 **Figure 4. Distinct geomorphological features related to coastal depositional/erosional features. The location of each panel is shown in Figure 3A. Elevation data from 1-meter DEMs (US Geological Survey, 2022).**

The transition to Pleistocene sedimentary units occurs south of these higher and presumably older units, where the curvilinear landforms, which range from 30 to 38m (NAVD88), are better preserved and of higher relief (Figure 4B, Figure 3A); an 260 erosional scarp oriented SW-NE at the base of this unit occurs at an elevation of 20m (NAVD88). The same scarp extends to the southwest (Figure 4C) with the presence of the landform whose interpretation as a sandbar was supported by Donoghue et al. (1998) but questioned by Otvos (1995). Revisiting these contrasting interpretations with higher-resolution elevations based on LIDAR surveys seems to confirm Donoghue's theory: younger features suggesting the presence of barriers were observed in lower elevations on both sides of the Apalachicola River (Figure 4D, E, F). Seaward concave features (Figure 4D) 265 resembling delta fronts (Olariu and Bhattacharya, 2006) appear on the east side of the Apalachicola River with high-relief barriers at elevations of 9.5-10m and 7-7.5m and wide flat areas (base - Figure 4D) at 7.5-8m and 6m respectively (NAVD88). South of these features, cuspate forelands dipping southwards are apparent (Supplementary Figure 1). On the west side of the river, sand barrier-like features have crest tops at +6m average elevation, while the surrounding base lies at +5m (NAVD88, Figure 4E). To the NW, these features continue but at increasing elevations, reaching a maximum crest elevations of +9m and

base elevation at +7m (NAVD88) (Figure 3A, Figure 4F), with a characteristic spit-end feature (Figure 4F) at the northeast end. On the eastern side, both sides of the Ochlockonee River have evidence of erosional scarps and spit-barrier features; the features on the river's east side are more prominent (Figure 4G) and have barrier crests from +8-10.5m and a scarp carved at +5m (NAVD88).

Immediately inland of the Holocene coastal barriers, a series of older Pleistocene strandplains are present in the Apalachicola area. The ones closest to the Holocene sequence were attributed to the Last Interglacial (MIS 5e, 125 ka, Burdette et al., 2012); the existence of deposits dating to previous Interglacials (MIS7,9) or to the MIS6 lowstand in the broader Apalachicola area (*Qu* formation in Figure 3A) was excluded by Otvos (1992) but supported by Donoghue et al., (1998). The only work providing radiometric ages for Pleistocene coastal sequences in this area is Burdette et al., (2012), who detected a MIS6 alluvium deposit and a fossiliferous nearshore fine-grained formation that was older than MIS6 (OSL saturated signal) and designated as *TQsu* on geological maps (Scott et al., 2001) and as the Biloxi formation by Otvos, 1992, shown as underlying the alluvium MIS6 deposit and the MIS5e beach ridges.

4. Methods

To characterize the subsurface stratigraphy of the most prominent Pleistocene beach barriers in the Apalachicola area, we collected 9 km of GPR data using a Sensors and Software EkkoPulse Pro using a 200 MHz antennae. Common-midpoint (CMP) surveys were conducted at each of our six GPR survey sites to determine the velocity of the radar waves within the subsurface. Velocities from these CMP surveys ranged from 0.043 to 0.082 m/ns. GPR profiles were topographically corrected using Global Navigation Satellite System (GNSS) survey data collected at the same time as the GPR. Processing of the GPR lines included automatic gain control and DeWow (a proprietary Sensors and Software processing algorithm). GPR profiles were loaded into EkkoView Deluxe software and ArcMap for interpretation. We assume that the vertical error associated with the identification of a point in the GPR profile is ±0.8m (1-sigma) based on the variability in radar velocities found throughout the area.

GNSS data were collected with a pair EMLID REACH RS+ receivers (single band) working in Real-Time-Kinematics (RTK) configuration. The position of the base station was initially set to uncorrected coordinates in the field and was corrected in post-processing using the FLCB permanent GNSS station (maintained by the Florida Department of Transportation, located 60-70km from our study area). All elevation data were referred to NAVD88 from the GNSS ellipsoid height using the online VDATUM tool by the US National Oceanic and Atmospheric Administration (https://vdatum.noaa.gov/vdatumweb/). Overall, we estimate that the vertical accuracy of this type of positioning is ±0.2m (1-sigma), including errors due to base postprocessing, rover-base positioning and vertical datum accuracy.

To reconstruct paleo relative sea level (RSL) from the Beach-Dune (BD) contact identified on GPR profiles, it is first necessary to quantify the position of sea level (and the associated uncertainty) at the time of formation of the BD contact---i.e. the indicative meaning (Shennan, 1986; Shennan et al., 2015). We quantify the BD contact indicative meaning by interpreting the modern beach-dune contact recognised on GPR profiles at three locations in the study area (Figure 5). Two are at Salinas Park on the east side of Cape San Blas (Lines 85 and 86, Figure 6A); the third is at a public beach access between Lafayette Drive and Martinique Drive on the west side of Cape San Blas (Line 83, Figure 6A). Altogether, these GPR profiles indicate that the BD contact is, on average, 0.92±0.46m (1-sigma) above modern sea level (Fig. 5B).

Using these values to determine the indicative meaning following Rovere et al., 2016, we calculate that the reference water level for beach-dune contacts in the area (i.e., the midpoint of the indicative range) is 0.92m and half of the indicative range, i.e., the uncertainty associated with the paleo RSL calculation, is 0.46m. These calculations mean that to calculate paleo relative sea level (RSL), 0.92m must be subtracted from the elevation of a BD contact point. The uncertainty of paleo RSL equals to the square root of the sum of squares of i) half of the indicative range (0.46m), ii) GPR vertical error (0.8m), and iii) GNSS error (0.2m). The total error associated with paleo RSL is therefore ±0.94m (1-sigma).

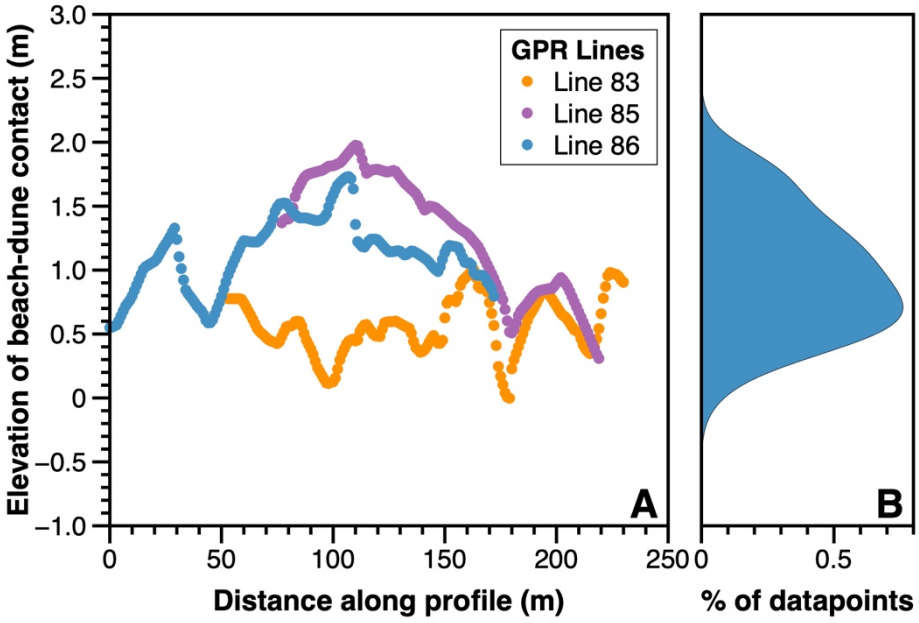

Figure 5 A) Beach-Dune contact identified along GPR lines across the modern shoreline. B) Density plot of the Beach-Dune contact at the three sites. Elevations are referred to the NAVD88 vertical datum.

5. Results and discussion

Based on the OSL dates acquired by Burdette et al., 2012 from the beach ridges of the tombolo-like formation (Figure 6B), the surficial beach ridges surveyed by our GPR lines belong to an age group with an average age of 114±9 ka BP, which overlies older beach deposits with an average age of 132±12 ka BP (Figure 6B). Considering these two age groups, we interpreted the age of the surficial strandplains identified on the DEM as shown in Fig.6. In our interpretation, we identify two distinct periods of beach ridge strandplain progradation. The younger one ranges in elevation from 0 to 4.5m and, due to its position relatively close to the modern coast -and the correlation with the OSL ages of Burdette et al. (2012)- we propose that it formed in late MIS5e. MIS 6 deposits were dated by Burdette et al., 2012 below marine/coastal sediments associated with a second, more landward ridge (Figure 6); we therefore propose that this older formed during early MIS 5e. Another relict strand plain, further inland, ranges in elevation from 4.3m to 8.5m and its planar geometry shows that it is disconnected from the two seaward barriers described above (Figure 6). We suggest that this strandplain, surveyed in GPR line L91 (Figure 6), is older than the Last Interglacial and may represent the imprint of a former highstand (MIS7, MIS 9 or MIS11). In the following text, we explore this hypothesis, while noting that an early MIS 5e age for the ridge cannot be excluded *a priori* without radiometric ages.

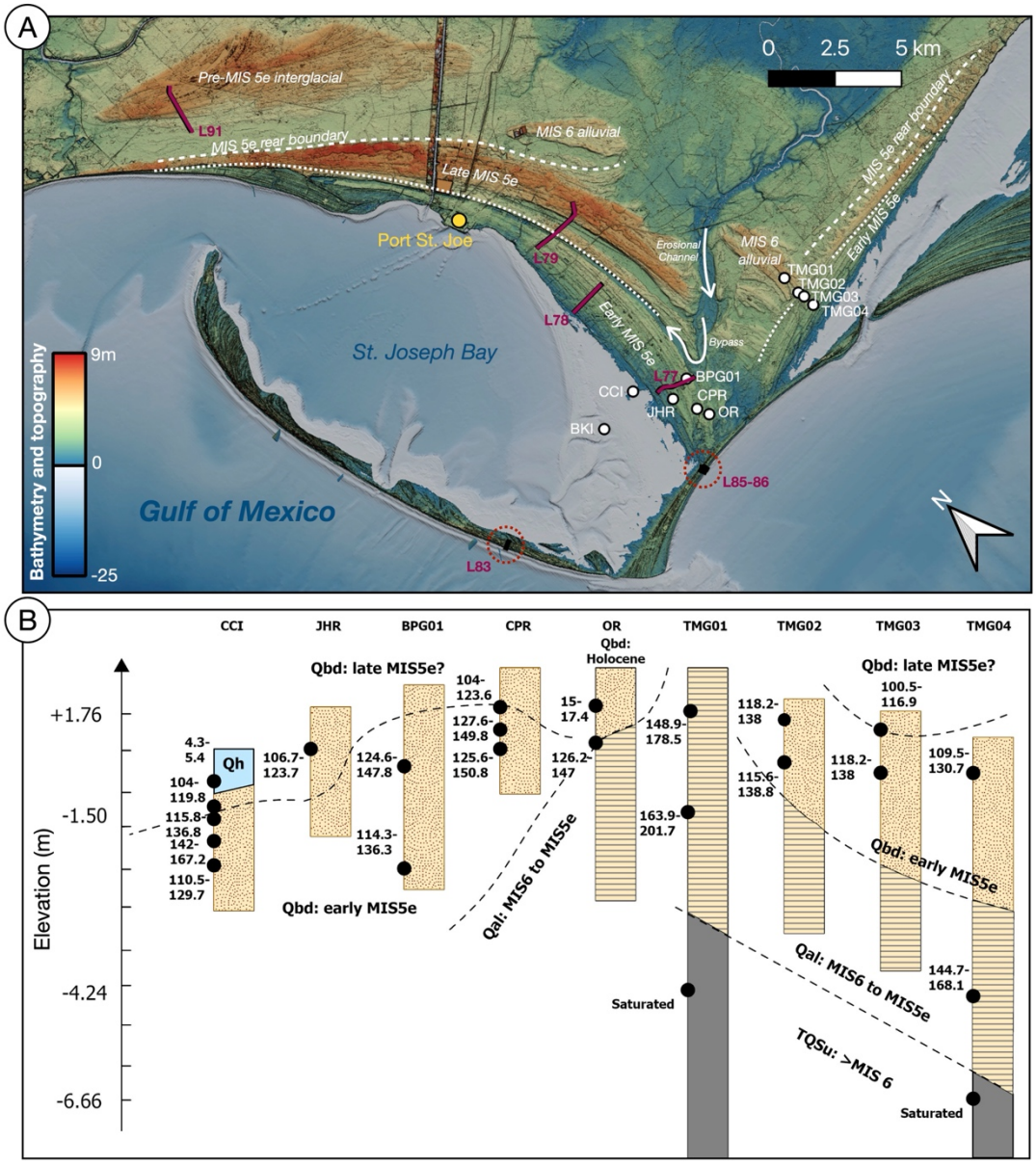

335 **Figure 6 A) Interpretation of Apalachicola's beach ridge system ages, and correlation with sediment cores from Burdette et al., 2012 (reproduced in Panel B). Elevation data from 1-meter DEMs and bathymetry from NOAA (NOAA National Centers for Environmental Information, 2023; US Geological Survey, 2022).**

5.1 Ground Penetrating Radar Stratigraphy

From the GPR profiles, we mapped a change in elevation of the beach-dune (BD) contact through the ridges that we interpret 340 to be MIS 5e in age. We crossed these ridges with three GPR lines: L77, L78 and L79 (Figure 6). L79 contains prograding beach deposits (Figure 7, A-A' profile) where the BD contact crosses both Early and Late MIS5e units. We identified an abrupt

drop of 4.5m at the BD contact, from a maximum height of 6.3m down to 1.8m (NAVD88, Supplementary GPR-L79). An alluvial cover is overlying the dipping beach deposits, while seaward the BD contact rises again reaching a maximum elevation of 3.9m. The BD contact appears to be continuously dropping until it reaches the current sea level with a 2 mm per meter of prograding beach (Supplementary GPR-L78).

A major feature interrupting the prograding beach deposits is an alluvial infill whose origin is linked to a sediment bypass feature (Nienhuis et al., 2016) observed at the beginning of L77. Sediment bypass features usually form when waves approach a river mouth obliquely, setting up a longshore current that transports more sediment along the coast than is brought ashore. Based on L78, the continuity of the beach deposits is interrupted by flat-lying tangent horizons that we interpret as erosional storm scarps (Figure 7, B-B' profile). L77 is less clear since it is affected by fluvial and wave erosion as observed on both east and west sides of the profile (Supplementary GPR-L77).

Farther north, within the stratigraphically older unit we tentatively assign to an interglacial preceding MIS 5e (Figure 7), seaward prograding beach deposits were detected in L91, with the BD contact found at a nearly constant elevation of 5.9m for 1km and gradually receding down to 2.6m after 0.9km of progradation (Supplementary GPR-L91). Erosional features that we attribute to storm events are also apparent in this unit (Figure 7, C-C' profile), similar to GPR-L78. Tracing L91 from south (C) to north (C'), an extended erosional surface interrupts the beach progradation at line distance ~360m, followed by a zone of hyperbolic reflections, suggesting a different depositional environment (Supplementary GPR-L91).

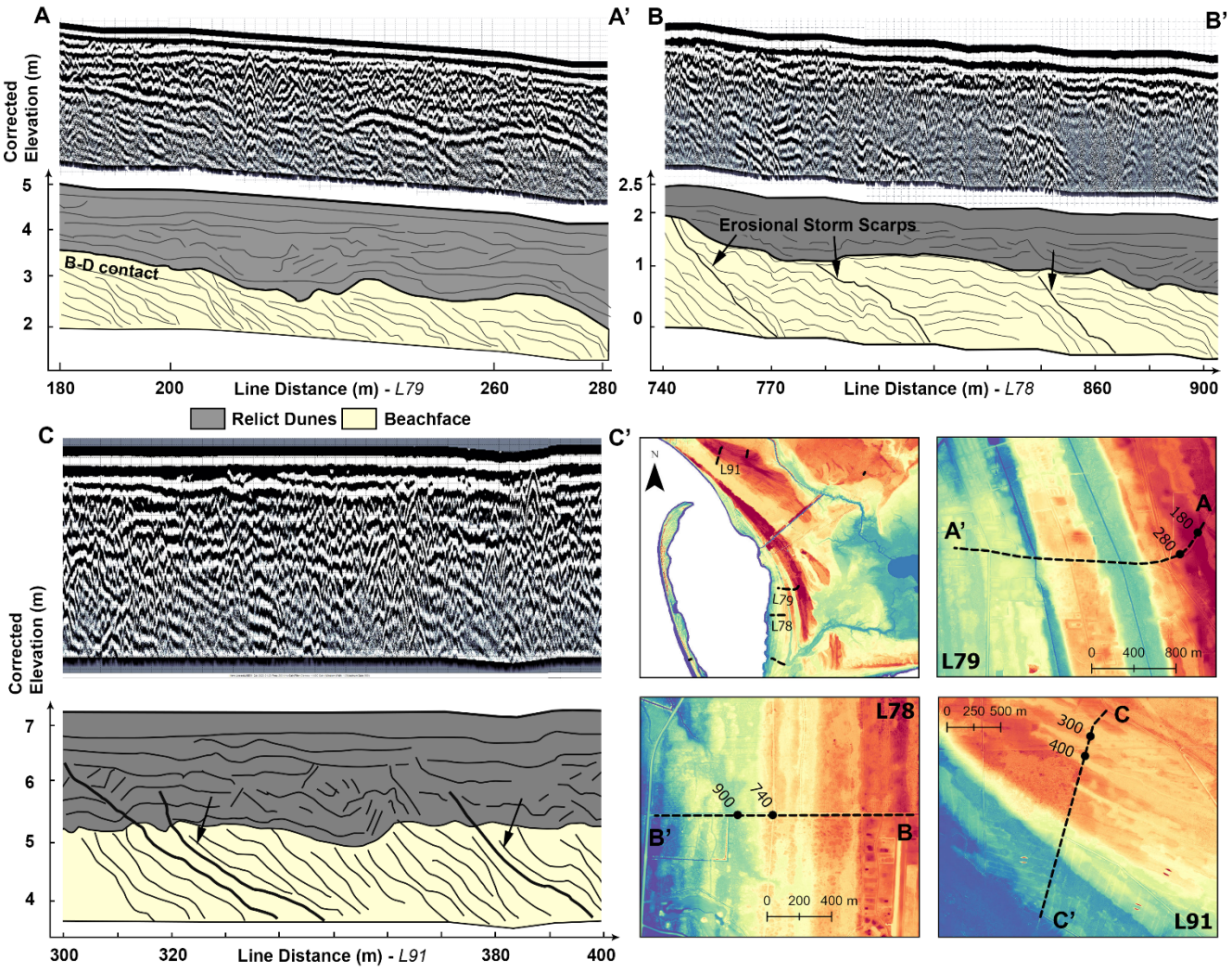

Figure 7 Location of GPR profiles and interpretation for GPR lines L79, L78, and L91. The profile locations are plotted on top of the 1-meter resolution DEMs (US Geological Survey, 2022).

5.2 Barrier progradation rates

The GPR profiles represent snapshots in time during past Pleistocene highstands. However, without radiometric ages in correspondence to the GPR profiles, it is challenging to establish the precise timing of Apalachicola coastal progradation. To overcome this issue, we turn to published Holocene barrier progradation rates in the area (Forrest, 2007; Rink and López, 2015, 2010). These rates were recalculated from the data reported by these authors (Table 1). Averaging only the long-term rates (>1 ka), we find that the average barrier progradation rate is 1.18±0.11 m/yr.

Table 1. Progradation rates from cores and associated OSL ages in the Holocene Apalachicola barrier island complex. For full information on the ages, see the source references. Progradation rates were obtained by dividing the distance between two cores and the average ages; errors were propagated considering age uncertainties. * indicates the records used for the average reported in the table's last row. † indicates the lowest progradation rate in the study area.

Location	Source	Age max (yrs)	Age min (yrs)	Distance (m)	Progradation rate (m/yr)
St Vincent Island*	Rink and López, 2010	1890±290	410±60	1300	0.88±0.18
Little St. George Island*	Rink and López, 2010	1900±200	500±50	3050	2.18±0.32
Little St. George Island	Rink and López, 2010	500±50	32±3	1200	2.56±0.27
Little St. George Island*	Rink and López, 2010	1900±200	32±3	4250	2.28±0.24
Cape San Blas	Rink and López, 2015	630±40	330±20	790	2.63±0.39
Cape San Blas	Rink and López, 2015	330±20	0	1400	4.24±0.26
Cape San Blas	Rink and López, 2015	630±40	0	2190	3.48±0.22
St. Joseph Peninsula	Rink and López, 2010	250±20	0	615	2.46±0.20
St. Joseph Peninsula	Rink and López, 2010	600±50	250±20	2419	6.91±1.06
Richardson Hammock	Rink and López, 2010	3300±300	3100±300	450	2.25
St Vincent Island	Forrest, 2007	4100±300	3500±300	2555	4.26±3.01
St Vincent Island*†	Forrest, 2007	3500±300	2500±200	682	0.68±0.25
St Vincent Island*	Forrest, 2007	2500±300	1200±100	1350	1.04±0.25
St Vincent Island	Forrest, 2007	1200±100	800±100	852	2.13±0.75
St Vincent Island	Forrest, 2007	800±100	400	816	2.04±0.51
St Vincent Island	Forrest, 2007	400	0	775	1.94
Weighted mean rates (and associated error) for periods longer than 1000 years					**1.18±0.11**

5.3 Pleistocene relative sea level changes

From the descriptions above, GPR profiles L78, L79 and L91 preserved the clearest and most continuous evidence of the Beach-Dune (BD) contact. Applying the relationship between the modern BD contact and sea level shown in Figure 5 to the elevation of the BD contact along these profiles and using a progradation rate of 1.18±0.11 m/yr (Table 1), it is possible to reconstruct relative sea level (RSL) changes within different periods throughout the late Pleistocene. Overall, the most striking features are the suggested RSL oscillations identified in the GPR profiles.

Using the progradation rate of 1.18 m/yr, GPR Line 91 runs through a beach barrier interpreted to have formed during an interglacial older than MIS 5e and represents a period of ~2000 years. RSL remains stable for about one millennium before falling at 5.8±0.5 mm/yr (Figure 8A). Higher sea-level fall rates are derived from GPR Line 79 (Figure 8B), which we correlate

to early MIS 5e. Starting from a peak RSL of ~5m, like the initial RSL in GPR Line 91, RSL drops at a rate of 14.3 mm/yr, then rises rapidly to 4m above present (Figure 8B). Sea level then falls again at 8.7 mm/yr (Figure 8B). Based on the progradation rates in Table 1, the oscillation happened in ~1200 years. GPR Line 78 indicates a more gradual sea-level fall (2.6 mm/yr), leading to the end of the LIG (Figure 8C). As these calculations depend on a mapping of Holocene rates to LIG rates, we explore adjusting the progradation rate to match the slowest rates measured in the Holocene (0.68 mm/yr). This adjustment leads to a modest modification of the RSL change rates (Figure 8B): at GPR Line 79, sea level would fall at 8.3 mm/yr, followed by a rise at 6 mm/yr and a successive fall at a rate of 5 mm/yr. At GPR Line 78, sea level would gradually fall at 1.5 mm/yr (Figure 8C).

Without a precise age assignment for this ridge, it is prudent to remain cautious in speculating about the origins of the MIS-5e RSL oscillation that we propose. Nevertheless, the rates of RSL change that we infer, and their relative age based on stratigraphic superposition, enable us to weigh several possible origins. First, the RSL oscillation could be caused by the isostatic response to sediment loading and unloading of the shelf during phases of increased or decreased sedimentation from the Apalachicola River delta. Sediment isostasy is capable of driving departures from eustasy of several meters between the present interglacial and the LIG (Pico, 2020), in particular in areas with rapid sedimentation such as the northern Gulf of Mexico. However, land motion rates calculated for LIG (Simms et al., 2013) and Holocene (Kuchar et al., 2018) shorelines are too low to fully explain the swings suggested by our GPR data.

Next, we consider ice sheet melt and glacial isostatic adjustment as origins for the Apalachicola RSL oscillation. Because the Apalachicola Delta sits on the Laurentide Ice Sheet's peripheral bulge, RSL there is sensitive to solid Earth effects associated with Laurentide melt as well as the fingerprints of Antarctic and Greenland excess melt. Antarctic Ice Sheet reconstructions during MIS-5e consistently find excess melt of >3m global mean sea level equivalent prior to 126 ka (Barnett et al., 2023; Golledge et al., 2021; Kopp et al., 2009), a contribution supported by evidence that the West Antarctic Ice Sheet collapsed during MIS-5e (Lau et al., 2023) and prior to 126 ka (Wolff et al., 2025), accompanied by substantial East Antarctic melt (Iizuka et al., 2023).

Early MIS-5e Antarctic collapse was likely accompanied by delayed Northern Hemisphere ice sheet melt. Mounting evidence supports Laurentide remnants persisting into early MIS-5e. For example, North Atlantic red layers dated to ~125-6 ka (Nicholl et al., 2012; Zhou and McManus, 2022) resemble cores of ~8.2 ka age deposited when a proglacial lake burst through the Laurentide and flooded the Labrador Sea (Jennings et al., 2015; Kerwin, 1996). These cores imply an outburst flood at ~125-6 ka similar to the 8.2 ka event flood, which requires a Laurentide of ~3+m GMSL equivalent volume (Zhou and McManus, 2022) and aligns with Labrador Sea isotope data showing glacial erosion of the Canadian craton through 126 ka (Parker and Harrison, 2022). An early MIS-5e Laurentide would have cooled the Northern Hemisphere (Hirose et al., 2025) despite high insolation forcing (Quiquet and Roche, 2024) and would help explain lower-than-present Norwegian Sea sea surface

temperatures (SST) from 128 - 126.5 ka (Ezat et al., 2024); freshwater plumes and iceberg rafted debris leaving the Labrador Sea at ~126 ka (Irvalı et al., 2016, 2012); and early MIS-5e SST proxies that lag behind ice volume proxies in the North Atlantic (Cline et al., 1984). Similarly, nearly all MIS-5e Greenland Ice Sheet volume estimates from the last decade place the ice sheet's peak contribution at 1-3 m GMSL equivalent after ~125 ka, in sync with the Northern Hemisphere summer insolation maximum at ~122 ka (Creel and Austermann, 2025).

The melting and regrowing of Earth's ice sheets at different times during MIS-5e could have contributed to an oscillation in Apalachicola RSL both through changes in GMSL and through glacial isostatic adjustment, which describes the viscoelastic response of the solid Earth to changes in ice and water loading (Farrell and Clark, 1976). When out of phase, ice sheet contributions to GMSL can mask each other (Raymo et al., 2006). Thus, whether MIS-5e GMSL oscillated by <1m (Dyer et al., 2021) or <4m (Kopp et al., 2013), much larger fluctuations in individual ice sheets could have occurred so long as the timing of peak melt varied. And because of the differing sea level fingerprints of each ice sheet (Hay et al., 2014), these ice sheet asymmetries could have led to rapid fluctuations in Apalachicola sea level.

Even without GMSL changes, the glacial isostatic adjustment (GIA) associated with asymmetric MIS-5e ice sheet melt could have led to a multi-meter oscillation in local sea level in the Gulf of Mexico (Creel and Austermann, 2025, Figure 8D). Creel and Austermann (2025) built an ensemble of ice sheet simulations in which simultaneous early MIS-5e Laurentide persistence and West Antarctic collapse balance to yield constant interglacial global mean sea level. We used this ensemble to find that because of GIA, simultaneous early MIS-5e Laurentide persistence and West Antarctic collapse can cause Apalachicola RSL to rise by 20+ mm/yr (early MIS-5e), then fall by up to -2 mm/yr, then rise by +2 mm/yr, then fall by 3-5+ mm/yr in late MIS-5e (Figure 8D). These rates, when compared to our RSL change rates inferred from GPR, have the right sign sequence but lower magnitude. This suggests that the concurrent but asymmetric melt and regrowth of multiple ice sheets may be needed to explain the rapid RSL changes we observe.

The most probable candidate for rapid melt and regrowth is the West Antarctic Ice Sheet (WAIS), for two reasons. First, each 1 mm/yr of WAIS melt/regrowth would increase/decrease Apalachicola RSL by ~1.3 mm/yr due to the fingerprint of WAIS ice melt (Hay et al., 2014). Second, WAIS collapse in early MIS-5e was likely triggered by ocean forcing (Clark et al., 2020). Once that warm water incursion abated, the low insolation during austral summer would have enabled some sectors of WAIS to regrow rapidly, as is suggested by the presence of the Ronne Ice Shelf by 126 ka (Wolff et al., 2025). The overlapping effects of WAIS regrowth, Laurentide Hudson Bay ice saddle collapse during the MIS-5e proglacial lake flooding event (Zhou and McManus, 2022), and concurrent Greenland melt (Yau et al., 2016), could have summed to rates of RSL change similar to the changes we record at Apalachicola. This scenario would also better align the Apalachicola RSL rates with MIS-5e sea-level rates reported in the Red Sea (Rohling et al., 2019, Figure 8E), as the Red Sea WAIS fingerprint is ~75% that of Apalachicola (Hay et al., 2014).

Besides the RSL oscillating pattern, in the latter part of GPR Line 78, we identified a sequence of seven erosional features that we interpreted as storm reflectors (Figure 7, Figure 8C). From our timing considerations, these seven erosional features were created during the very last part of MIS 5e (i.e., around 113-117 ka, Figure 8E). Considering the progradation rate of 1.18 m/yr, these storms happened over a period of ~540 years. This translates into a recurrence of one major storm every 76 years in the last part of MIS 5e. This is a lower frequency of extreme events than the historical one (one every 42 years, Rodysill et al., 2020), but higher than the minimum value of 12 extreme hurricanes in ~2500 years proposed for the Gulf of Mexico by Bregy et al., 2018. This discrepancy might reflect the fact that the vertical resolution of the GPR may only capture events above a certain magnitude threshold (e.g., hurricane category ≥3), or that beach ridge formation is influenced primarily by such high-intensity events, whereas sediment cores may preserve a broader range of storm imprints.

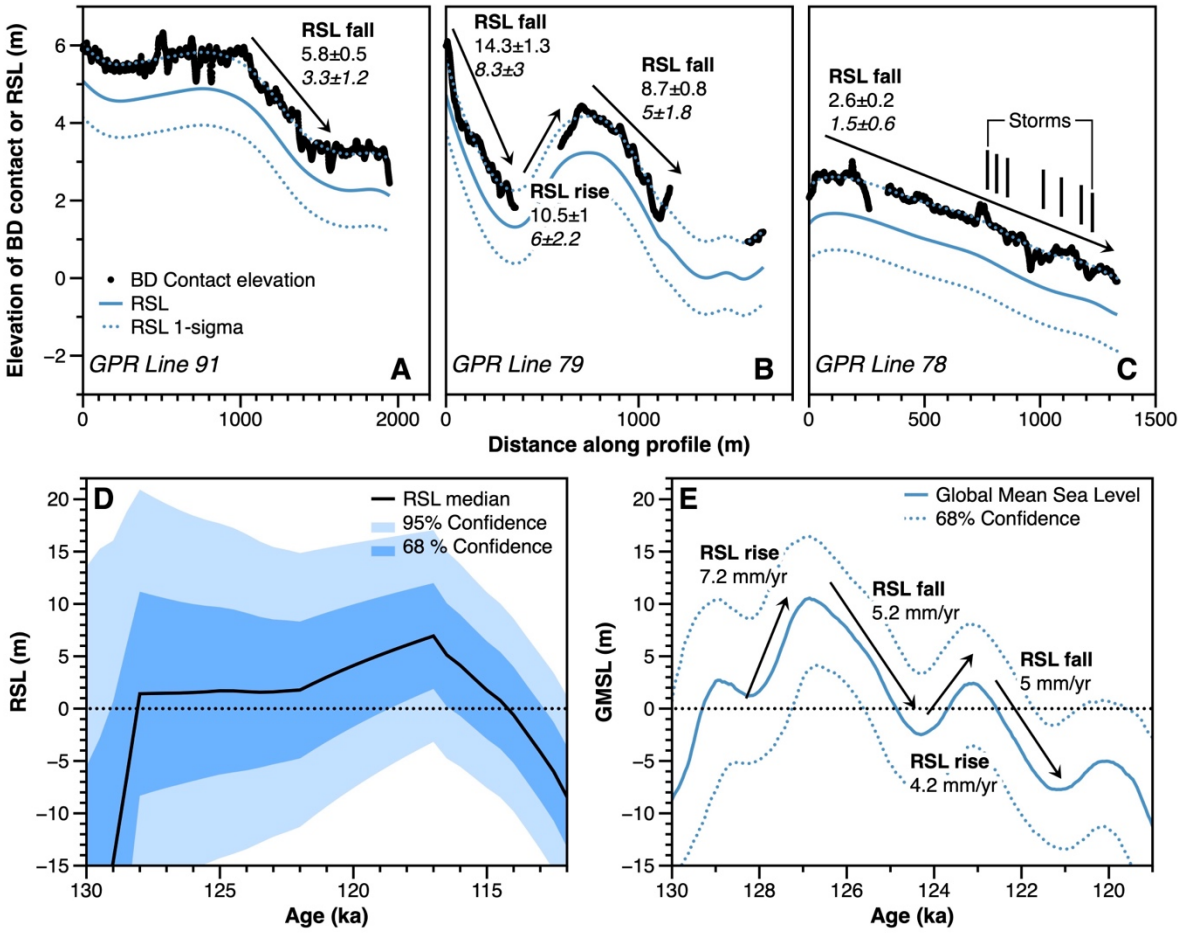

Figure 8. A) Beach-Dune contact and associated RSL at GPR Line 91, interpreted as pre-MIS 5e (see text for discussion). B) and C) Same as A), but for GPR Lines 79 and 78, respectively representative of early / mid and late MIS 5e (see text for discussion). D) GIA relative sea level as predicted by glacial isostatic adjustment models at Cape San Blas (Creel and Austermann, 2025). F) GMSL during MIS 5e and associated rates as calculated by Rohling et al., 2019.

5.4 Paleogeographical evolution of the Apalachicola Barrier Island Complex

To reconstruct the evolution of the Apalachicola coastal barrier system, our results suggest that an extended coastal barrier system prograded during the early highstand of MIS 5e forming east-west oriented barrier islands and a north-south oriented strandplain attached to its west to Pleistocene bedrock (Figure 9A). During the MIS5e RSL fall (Figure 9B), the ancestral Apalachicola River prograded, eroding the strandplain and seabed near Cape San Blas and forming the modern-day channel of Depot Creek – which now flows to the north but whose tributaries appear to indicate a southward directed flow at one time (Donoghue, 1993). After sea level rose in the Late MIS5e, the small river in Cape San Blas was bypassed and younger beach ridges formed attached to the Late MIS5e unit (Figure 9C). Finally, during the Holocene transgression new smaller barrier islands formed south of the Pleistocene coastal barrier system. These islands, located along Cape San Blas, connected to the Pleistocene units as the Apalachicola River now rerouted to enter the Gulf eastward of its late MIS5e location (Figure 9D).

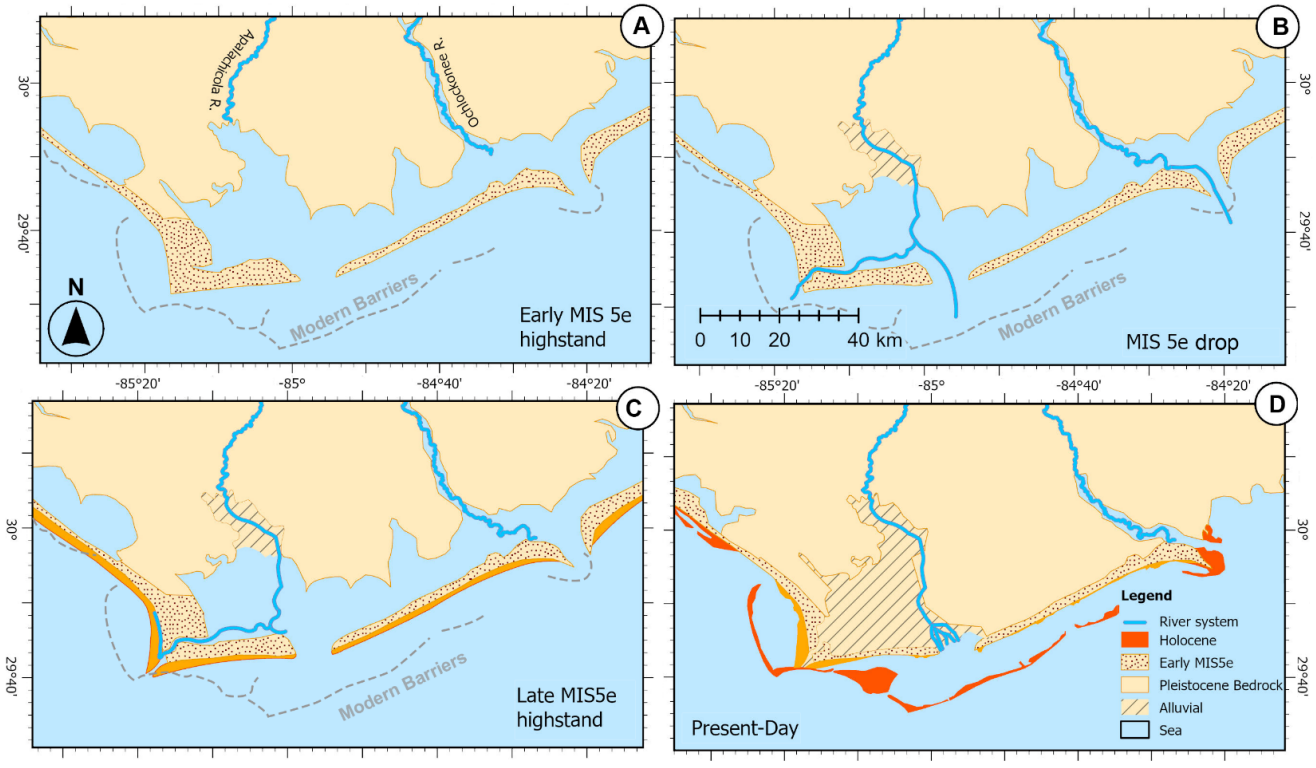

Figure 9. Evolution of the Apalachicola coastal barrier system since the Last Interglacial (MIS5e). A) Early MIS 5e highstand; B). MIS5e drop, C) Late MIS5e highstand, D) Present-day coastal morphology.

6. Conclusions

We acquired new Ground Penetrating Radar (GPR) profiles and RTK measurements across modern and fossil beach ridges and strandplains in the Apalachicola River Delta area of northwest Florida. Combined with existing LiDAR-derived digital

elevation models (DEMs) and Optically Stimulated Luminescence (OSL) dates, these data provide new insights into the region's response to sea-level changes over geological timescales. Based on this integrated analysis, we propose a coastal barrier evolution model for the broader Apalachicola Delta area from the Last Interglacial (MIS 5e) to the present. Our results show that marine deposits extend across the Apalachicola Delta from elevations as high as +75 meters (NAVD88) down to mean sea level, likely representing sedimentation from the Late Pliocene to Early Pleistocene. Coastal landforms such as spits, barriers, and sandbars were recognized, attesting to the long and dynamic coastal history of the area.+

Within the Pleistocene coastal sequences, GPR, LiDAR, and OSL data reveal the existence of two distinct beach ridge units formed during the early and late phases of MIS 5e. These units appear to have been shaped by rapid sea-level oscillations. The rates of relative sea-level change recorded exceed those expected from glacial isostatic adjustment or local sedimentary processes alone. We therefore propose that the observed oscillations are linked to the regrowth of a collapsed West Antarctic Ice Sheet, coinciding with ongoing Laurentide and Greenland ice melt during MIS 5e. Further inland, we identified a third, stratigraphically older beach ridge plain, likely formed during a previous interglacial period (MIS 7, or older), although an early MIS 5e age cannot be definitively excluded. The presence of MIS 6 alluvial deposits and better-preserved coastal sequences in the western delta supports the interpretation of a complex, multi-phase Pleistocene evolution.

Additionally, erosional scarps identified in GPR profiles suggest the occurrence of major storm events approximately every 76 years during the latter part of MIS 5e, highlighting the dynamic interplay between storm activity and barrier development; however, this estimate is tentative, as it depends on assumptions about GPR resolution and the preservation of only higher-magnitude events.

Supplementary Information

All data and supplementary figures mentioned in the text are available open-access at this link: https://doi.org/10.5281/zenodo.15202796

A preprint of this manuscript was submitted on May 4th, 2025 to EarthArXiv.

Acknowledgements

This work was funded by the European Research Council (ERC) under the European Union's Horizon 2020 research and innovation programme (grant agreement n. 802414). The manuscript reflects only the view of the authors and the EU is not responsible for any use that may be made of the information it contains. RC was supported by a Woods Hole Oceanographic Institution Postdoctoral Scholarship'.

References

Andrade, A.C.S., Dominguez, J.M.L., Martin, L., Bittencourt, A.C.S.P., 2003. Quaternary evolution of the Caravelas strandplain - Southern Bahia State - Brazil. An. Acad. Bras. Ciênc. 75, 357–382. https://doi.org/10.1590/S0001-37652003000300008

Barnett, R.L., Austermann, J., Dyer, B., Telfer, M.W., Barlow, N.L., Boulton, S.J., Carr, A.S., Creel, R.C., 2023. Constraining the contribution of the Antarctic Ice Sheet to Last Interglacial sea level. Sci. Adv. 9, eadf0198.

Boyd, R., Dalrymple, R., Zaitlin, B., 1992. Classification of clastic coastal depositional environments. Sediment. Geol. 80, 139–150.

Bregy, J.C., Wallace, D.J., Totten, R.L., Cruz, V.J., 2018. 2500-year paleotempestological record of intense storms for the northern Gulf of Mexico, United States. Mar. Geol. 396, 26–42. https://doi.org/10.1016/j.margeo.2017.09.009

Brenneman, L., Tanner, W.F., 1958. Possible abandoned barrier islands in panhandle Florida. J. Sediment. Res. 28, 342–344.

Burdette, K.E., Rink, W.J., López, G.I., Mallinson, D.J., Parham, P.R., Reinhardt, E.G., 2012. Geological investigation and optical dating of Quaternary siliciclastic sediments near Apalachicola, North-west Florida, USA. Sedimentology 59, 1836–1849. https://doi.org/10.1111/j.1365-3091.2012.01328.x

Buynevich, I.V., FitzGerald, D.M., Goble, R.J., 2007. A 1500 yr record of North Atlantic storm activity based on optically dated relict beach scarps. Geology 35, 543–546.

Carruthers, E.A., Lane, D.P., Evans, R.L., Donnelly, J.P., Ashton, A.D., 2013. Quantifying overwash flux in barrier systems: An example from Martha's Vineyard, Massachusetts, USA. Mar. Geol. 343, 15–28.

Carvalho, R.C., Oliver, T.S.N., Woodroffe, C.D., 2019. Transition from marine to fluvial-dominated sediment supply at Shoalhaven prograded barrier, southeastern Australia. Geomorphology 341, 65–78. https://doi.org/10.1016/j.geomorph.2019.05.010

Ciarletta, D.J., Shawler, J.L., Tenebruso, C., Hein, C.J., Lorenzo-Trueba, J., 2019. Reconstructing coastal sediment budgets from beach-and foredune-ridge morphology: A coupled field and modeling approach. J. Geophys. Res. Earth Surf. 124, 1398–1416.

Clark, P.U., He, F., Golledge, N.R., Mitrovica, J.X., Dutton, A., Hoffman, J.S., Dendy, S., 2020. Oceanic forcing of penultimate deglacial and last interglacial sea-level rise. Nature 577, 660–664.

Clifton, H.E., 2005. Coastal Sedimentary Facies, in: Schwartz, M.L. (Ed.), Encyclopedia of Coastal Science. Springer Netherlands, Dordrecht, pp. 270–278. https://doi.org/10.1007/1-4020-3880-1_84

Cline, R.M.L., Hays, J.D., Prell, W.L., Ruddiman, W.F., Moore, T.C., Kipp, N.G., Molfino, B.E., Denton, G.H., Hughes, T.J., Balsam, W.L., Brunner, C.A., Duplessy, J.-C., Esmay, A.G., Fastook, J.L., Imbrie, J., Keigwin, L.D., Kellogg, T.B., McIntyre, A., Matthews, R.K., Mix, A.C., Morley, J.J., Shackleton, N.J., Streeter, S.S., Thompson, P.R., 1984. The Last Interglacial Ocean. Quat. Res. 21, 123–224. https://doi.org/10.1016/0033-5894(84)90098-X

Costas, S., Ferreira, Ó., Plomaritis, T.A., Leorri, E., 2016. Coastal barrier stratigraphy for Holocene high-resolution sea-level reconstruction. Sci. Rep. 6, 38726. https://doi.org/10.1038/srep38726

Creel, R.C., Austermann, J., 2025. Glacial isostatic adjustment driven by asymmetric ice sheet melt during the Last Interglacial causes multiple local sea-level peaks. Geology 53, 253–258. https://doi.org/10.1130/G52483.1

Donnelly, C., Kraus, N., Larson, M., 2006. State of knowledge on measurement and modeling of coastal overwash. J. Coast. Res. 22, 965–991.

Donoghue, J.F., Stapor, F.W., Tanner, W.F., 1998. Discussion of: Otvos, EG, 1995. Multiple Pliocene-Quaternary Marine Highstands, Northeast Gulf Coastal Plain-Fallacies and Facts. Journal of Coastal Research, 11, 984-1002. J. Coast. Res. 669–674.

Dougherty, A.J., 2018. Prograded coastal barriers provide paleoenvironmental records of storms and sea level during late Quaternary highstands. J. Quat. Sci. 33, 501–517.

Dyer, B., Austermann, J., D'Andrea, W.J., Creel, R.C., Sandstrom, M.R., Cashman, M., Rovere, A., Raymo, M.E., 2021. Sea-level trends across the Bahamas constrain peak last interglacial ice melt. Proc. Natl. Acad. Sci. U. S. A. 118, 1–11. https://doi.org/10.1073/pnas.2026839118

Ezat, M.M., Fahl, K., Rasmussen, T.L., 2024. Arctic freshwater outflow suppressed Nordic Seas overturning and oceanic heat transport during the Last Interglacial. Nat. Commun. 15, 8998. https://doi.org/10.1038/s41467-024-53401-3

Fairbridge, R.W., Hillaire-Marcel, C., 1977. An 8,000-yr palaeoclimatic record of the 'Double-Hale'45-yr solar cycle. Nature 268, 413–416.
Farrell, W., Clark, J.A., 1976. On postglacial sea level. Geophys. J. Int. 46, 647–667.
Flemming, B., 1982. Xi. Beach morphodynamics in relationship to wave energy, grain size and internal sedimentary structure. Jt. Geol. Surv. Cape Town 97.
Forrest, B.M., 2007. Evolution of the beach ridge strandplain on st. Vincent island, florida (Ph.D. Thesis). The Florida State University.
Gernant, C., Simms, A.R., DeWitt, R., Theilen, B., Garcia, C.N., Goebel, M., 2025. Insights into the sea-level history of the South Shetland Islands from ground penetrating radar on Livingston Island, Antarctica. Quat. Sci. Rev. 359, 109363.
Goetschius, D.W., 1971. Preliminary sedimentological and geomorphological study of certain high terrace sands between the Ochlockonee and Apalachicola rivers, Liberty and Gadsden Counties, Florida (PhD Thesis). Florida State University.
Golledge, N.R., Clark, P.U., He, F., Dutton, A., Turney, C.S.M., Fogwill, C.J., Naish, T.R., Levy, R.H., McKay, R.M., Lowry, D.P., Bertler, N.A.N., Dunbar, G.B., Carlson, A.E., 2021. Retreat of the Antarctic Ice Sheet During the Last Interglaciation and Implications for Future Change. Geophys. Res. Lett. 48, e2021GL094513. https://doi.org/10.1029/2021GL094513
Goodwin, I.D., Mortlock, T.R., Ribo, M., Mitrovica, J.X., O'Leary, M., Williams, R., 2023. Robbins Island: The index site for regional Last Interglacial sea level, wave climate and the subtropical ridge around Bass Strait, Australia. Quat. Sci. Rev. 305, 107996.
Goodwin, I.D., Ribó, M., Mortlock, T., 2020. Coastal sediment compartments, wave climate and centennial-scale sediment budget, in: Sandy Beach Morphodynamics. Elsevier, pp. 615–640.
Goslin, J., Clemmensen, L.B., 2017. Proxy records of Holocene storm events in coastal barrier systems: Storm-wave induced markers. Quat. Sci. Rev. 174, 80–119. https://doi.org/10.1016/j.quascirev.2017.08.026
Hay, C., Mitrovica, J.X., Gomez, N., Creveling, J.R., Austermann, J., Kopp, R.E., 2014. The sea-level fingerprints of ice-sheet collapse during interglacial periods. Quat. Sci. Rev. 87, 60–69.
Hede, M.U., Bendixen, M., Clemmensen, L.B., Kroon, A., Nielsen, L., 2013. Joint interpretation of beach-ridge architecture and coastal topography show the validity of sea-level markers observed in ground-penetrating radar data. The Holocene 23, 1238–1246.
Hein, C.J., Ashton, A.D., 2020. Long-term shoreline morphodynamics: processes and preservation of environmental signals. Sandy Beach Morphodynamics 487–531.
Hesp, P.A., 1984. Foredune formation in southeast Australia, in: Coastal Geomorphology in Australia. Academic Press, pp. 69–97.
Hirose, L.A., Abe-Ouchi, A., Chan, W.-L., O'ishi, R., Yoshimori, M., Obase, T., 2025. Arctic Warming Suppressed by Remnant Glacial Ice Sheets in Past Interglacials. Geophys. Res. Lett. 52, e2024GL111798. https://doi.org/10.1029/2024GL111798
Holdahl, S.R., Morrison, N.L., 1974. Regional investigations of vertical crustal movements in the US, using precise relevelings and mareograph data. Tectonophysics 23, 373–390.
Iizuka, M., Seki, O., Wilson, D.J., Suganuma, Y., Horikawa, K., van de Flierdt, T., Ikehara, M., Itaki, T., Irino, T., Yamamoto, M., Hirabayashi, M., Matsuzaki, H., Sugisaki, S., 2023. Multiple episodes of ice loss from the Wilkes Subglacial Basin during the Last Interglacial. Nat. Commun. 14, 2129. https://doi.org/10.1038/s41467-023-37325-y
Irvalı, N., Ninnemann, U.S., Galaasen, E.V., Rosenthal, Y., Kroon, D., Oppo, D.W., Kleiven, H.F., Darling, K.F., Kissel, C., 2012. Rapid switches in subpolar North Atlantic hydrography and climate during the Last Interglacial (MIS 5e). Paleoceanography 27. https://doi.org/10.1029/2011PA002244
Irvalı, N., Ninnemann, U.S., Kleiven, H. (Kikki) F., Galaasen, E.V., Morley, A., Rosenthal, Y., 2016. Evidence for regional cooling, frontal advances, and East Greenland Ice Sheet changes during the demise of the last interglacial. Quat. Sci. Rev. 150, 184–199. https://doi.org/10.1016/j.quascirev.2016.08.029
Isla, M.F., Moyano-Paz, D., FitzGerald, D.M., Simontacchi, L., Veiga, G.D., 2023. Contrasting beach-ridge systems in different types of coastal settings. Earth Surf. Process. Landf. 48, 47–71.
Jennings, A., Andrews, J., Pearce, C., Wilson, L., Ólfasdótttir, S., 2015. Detrital carbonate peaks on the Labrador shelf, a 13–7ka template for freshwater forcing from the Hudson Strait outlet of the Laurentide Ice Sheet into the subpolar gyre. Quat. Sci. Rev. 107, 62–80. https://doi.org/10.1016/j.quascirev.2014.10.022

Jol, H.M., Smith, D.G., Meyers, R.A., 1996. Digital ground penetrating radar (GPR): a new geophysical tool for coastal barrier research (examples from the Atlantic, Gulf and Pacific Coasts, USA). J. Coast. Res. 960–968.
Kerwin, M.W., 1996. A Regional Stratigraphic Isochron (ca. 800014C yr B.P.) from Final Deglaciation of Hudson Strait. Quat. Res. 46, 89–98. https://doi.org/10.1006/qres.1996.0049
Komar, P.D., Wang, C., 1984. Processes of selective grain transport and the formation of placers on beaches. J. Geol. 92, 637–655.
Kopp, R.E., Simons, F.J., Mitrovica, J.X., Maloof, A.C., Oppenheimer, M., 2013. A probabilistic assessment of sea level variations within the last interglacial stage. Geophys. J. Int. 193, 711–716. https://doi.org/10.1093/gji/ggt029
Kopp, R.E., Simons, F.J., Mitrovica, J.X., Maloof, A.C., Oppenheimer, M., 2009. Probabilistic assessment of sea level during the last interglacial stage. Nature 462, 863–867. https://doi.org/10.1038/nature08686
Kuchar, J., Milne, G., Wolstencroft, M., Love, R., Tarasov, L., Hijma, M., 2018. The Influence of Sediment Isostatic Adjustment on Sea Level Change and Land Motion Along the U.S. Gulf Coast. J. Geophys. Res. Solid Earth 123, 780–796. https://doi.org/10.1002/2017JB014695
Kumar, R., Switzer, A.D., Gouramanis, C., Bristow, C.S., Shaw, T.A., Jankaew, K., Li, T., Brill, D., 2024. Late-Holocene sea-level markers preserved in a beach ridge system on Phra Thong Island, Thailand. Geomorphology 465, 109405.
Lau, S.C.Y., Wilson, N.G., Golledge, N.R., Naish, T.R., Watts, P.C., Silva, C.N.S., Cooke, I.R., Allcock, A.L., Mark, F.C., Linse, K., Strugnell, J.M., 2023. Genomic evidence for West Antarctic Ice Sheet collapse during the Last Interglacial. Science 382, 1384–1389. https://doi.org/10.1126/science.ade0664
Lindhorst, S., Schutter, I., 2014. Polar gravel beach-ridge systems: Sedimentary architecture, genesis, and implications for climate reconstructions (South Shetland Islands/Western Antarctic Peninsula). Geomorphology 221, 187–203.
Mammì, I., Rossi, L., Pranzini, E., 2019. Mathematical reconstruction of eroded beach ridges at the Ombrone River Delta. Water 11, 2281.
Masselink, G., Kroon, A., Davidson-Arnott, R.G.D., 2006. Morphodynamics of intertidal bars in wave-dominated coastal settings — A review. Geomorphology 73, 33–49. https://doi.org/10.1016/j.geomorph.2005.06.007
Masselink, G., van Heteren, S., 2014. Response of wave-dominated and mixed-energy barriers to storms. Mar. Geol. 352, 321–347.
Mauz, B., Hijma, M., Amorosi, A., Porat, N., Galili, E., Bloemendal, J., 2013. Aeolian beach ridges and their significance for climate and sea level: Concept and insight from the Levant coast (East Mediterranean). Earth-Sci. Rev. 121, 31–54.
Maxwell, R., 1971a. Preliminary ionium date from marine terrace, Florida. Coast. Res. Notes 3, 9–10.
Maxwell, R., 1971b. Origin and chronology of Alabama River terraces. GCAGS Trans.
Montes, A., Bujalesky, G.G., Paredes, J.M., 2018. Geomorphology and internal architecture of Holocene sandy-gravel beach ridge plain and barrier spits at Río Chico area, Tierra del Fuego, Argentina. J. South Am. Earth Sci. 84, 172–183.
Nicholl, J.A.L., Hodell, D.A., Naafs, B.D.A., Hillaire-Marcel, C., Channell, J.E.T., Romero, O.E., 2012. A Laurentide outburst flooding event during the last interglacial period. Nat. Geosci. 5, 901–904. https://doi.org/10.1038/ngeo1622
Nielsen, L., Bendixen, M., Kroon, A., Hede, M.U., Clemmensen, L.B., Weβling, R., Elberling, B., 2017. Sea-level proxies in Holocene raised beach ridge deposits (Greenland) revealed by ground-penetrating radar. Sci. Rep. 7, 46460.
Nienhuis, J.H., Ashton, A.D., Giosan, L., 2016. Littoral steering of deltaic channels. Earth Planet. Sci. Lett. 453, 204–214. https://doi.org/10.1016/j.epsl.2016.08.018
NOAA National Centers for Environmental Information, 2023. Coastal Relief Models. NOAA National Centers for Environmental Information. https://doi.org/10.25921/5ZN5-KN44
Nooren, K., Hoek, W.Z., Winkels, T., Huizinga, A., Van Der Plicht, H., Van Dam, R.L., Van Heteren, S., Van Bergen, M.J., Prins, M.A., Reimann, T., Wallinga, J., Cohen, K.M., Minderhoud, P., Middelkoop, H., 2017. The Usumacinta–Grijalva beach-ridge plain in southern Mexico: a high-resolution archive of river discharge and precipitation. Earth Surf. Dyn. 5, 529–556. https://doi.org/10.5194/esurf-5-529-2017
Okazaki, H., Nara, M., Nakazato, H., Furusawa, A., Ito, K., Tamura, T., 2022. Coastal progradation associated with sea-level oscillations in the later phase of the Last Interglacial period, central Japan. Quat. Sci. Rev. 285, 107507.
Olariu, C., Bhattacharya, J.P., 2006. Terminal distributary channels and delta front architecture of river-dominated delta systems. J. Sediment. Res. 76, 212–233.
Otvos, E.G., 2000. Beach ridges — definitions and significance. Geomorphology 32, 83–108. https://doi.org/10.1016/S0169-555X(99)00075-6

Otvos, E.G., 1995. Multiple pliocene-quaternary marine highstands, northeast Gulf Coastal plain: fallacies and facts. J. Coast. Res. 984–1002.
Otvos, E.G., 1992. Quaternary evolution of the Apalachicola coast, northeastern Gulf of Mexico.
Parker, S.E., Harrison, S.P., 2022. The timing, duration and magnitude of the 8.2 ka event in global speleothem records. Sci. Rep. 12, 10542. https://doi.org/10.1038/s41598-022-14684-y
Pedoja, K., Regard, V., Husson, L., Martinod, J., Guillaume, B., Fucks, E., Iglesias, M., Weill, P., 2011. Uplift of quaternary shorelines in eastern Patagonia: Darwin revisited. Geomorphology 127, 121–142. https://doi.org/10.1016/j.geomorph.2010.08.003
Phillips, M., Blenkinsopp, C., Splinter, K., Harley, M., Turner, I., 2019. Modes of berm and beachface recovery following storm reset: Observations using a continuously scanning lidar. J. Geophys. Res. Earth Surf. 124, 720–736.
Pico, T., 2020. Towards assessing the influence of sediment loading on Last Interglacial sea level. Geophys. J. Int. 220, 384–392. https://doi.org/10.1093/gji/ggz447
Pranzini, E., 2024. Airborne LIDAR survey applied to the analysis of the historical evolution of the Arno River delta (Italy). J. Coast. Res. 50, 400–409.
Quiquet, A., Roche, D.M., 2024. Investigating similarities and differences of the penultimate and last glacial terminations with a coupled ice sheet–climate model. Clim. Past 20, 1365–1385. https://doi.org/10.5194/cp-20-1365-2024
Raymo, M.E., Lisiecki, L.E., Nisancioglu, K.H., 2006. Plio-Pleistocene Ice Volume, Antarctic Climate, and the Global δ18O Record. Science 313, 492–495. https://doi.org/10.1126/science.1123296
Rink, W.J., López, G.I., 2015. Corrigendum to "OSL-based lateral progradation and aeolian sediment accumulation rates for the Apalachicola Barrier Island Complex, North Gulf of Mexico, Florida" [Geomorphology 123 (2010) 330–342]. Geomorphology 241, 41. https://doi.org/10.1016/j.geomorph.2015.02.016
Rink, W.J., López, G.I., 2010. OSL-based lateral progradation and aeolian sediment accumulation rates for the Apalachicola Barrier Island Complex, North Gulf of Mexico, Florida. Geomorphology 123, 330–342. https://doi.org/10.1016/j.geomorph.2010.08.001
Rodriguez, A.B., Meyer, C.T., 2006. Sea-level variation during the Holocene deduced from the morphologic and stratigraphic evolution of Morgan Peninsula, Alabama, USA. J. Sediment. Res. 76, 257–269.
Rodysill, J.R., Donnelly, J.P., Sullivan, R., Lane, P.D., Toomey, M., Woodruff, J.D., Hawkes, A.D., MacDonald, D., d'Entremont, N., McKeon, K., Wallace, E., Van Hengstum, P.J., 2020. Historically unprecedented Northern Gulf of Mexico hurricane activity from 650 to 1250 CE. Sci. Rep. 10, 19092. https://doi.org/10.1038/s41598-020-75874-0
Rohling, E.J., Hibbert, F.D., Grant, K.M., Galaasen, E.V., Irvalı, N., Kleiven, H.F., Marino, G., Ninnemann, U., Roberts, A.P., Rosenthal, Y., Schulz, H., Williams, F.H., Yu, J., 2019. Asynchronous Antarctic and Greenland ice-volume contributions to the last interglacial sea-level highstand. Nat. Commun. 10, 5040. https://doi.org/10.1038/s41467-019-12874-3
Rovere, A., Raymo, M.E., Vacchi, M., Lorscheid, T., Stocchi, P., Gómez-Pujol, L., Harris, D.L., Casella, E., O'Leary, M.J., Hearty, P.J., 2016. The analysis of Last Interglacial (MIS 5e) relative sea-level indicators: Reconstructing sea-level in a warmer world. Earth-Sci. Rev. 159, 404–427. https://doi.org/10.1016/j.earscirev.2016.06.006
Rubio-Sandoval, K., Ryan, D.D., Richiano, S., Giachetti, L.M., Hollyday, A., Bright, J., Gowan, E.J., Pappalardo, M., Austermann, J., Kaufman, D.S., Rovere, A., 2024. Quaternary and Pliocene sea-level changes at Camarones, central Patagonia, Argentina. Quat. Sci. Rev. 345, 108999. https://doi.org/10.1016/j.quascirev.2024.108999
Ruz, M.-H., Allard, M., 1994. Coastal dune development in cold-climate environments. Phys. Geogr. 15, 372–380.
Scheffers, A., Engel, M., Scheffers, S., Squire, P., Kelletat, D., 2012. Beach ridge systems–archives for Holocene coastal events? Prog. Phys. Geogr. 36, 5–37.
Schnable, J.E., Goodell, H.G., 1968. Pleistocene-Recent stratigraphy, evolution, and development of the Apalachicola coast, Florida. Geological Society of America.
Scott, T.M., Campbell, K.M., Rupert, F.R., Arthur, J.D., Missimer, T.M., Lloyd, J.M., Yon, J.W., Duncan, J.G., 2001. Geologic map of the state of Florida. Florida Geological Survey Tallahassee, Fla.
Shennan, I., 1986. Flandrian sea-level changes in the Fenland. II: Tendencies of sea-level movement, altitudinal changes, and local and regional factors. J. Quat. Sci. 1, 155–179. https://doi.org/10.1002/jqs.3390010205
Shennan, I., Long, A.J., Horton, B.P., 2015. Handbook of sea-level research. John Wiley & Sons.

Simms, A.R., Anderson, J.B., DeWitt, R., Lambeck, K., Purcell, A., 2013. Quantifying rates of coastal subsidence since the last interglacial and the role of sediment loading. Glob. Planet. Change 111, 296–308. https://doi.org/10.1016/j.gloplacha.2013.10.002

Stapor Jr, F.W., Mathews, T.D., Lindfors-Kearns, F.E., 1991. Barrier-island progradation and Holocene sea-level history in southwest Florida. J. Coast. Res. 815–838.

Stattegger, K., Tjallingii, R., Saito, Y., Michelli, M., Thanh, N.T., Wetzel, A., 2013. Mid to late Holocene sea-level reconstruction of Southeast Vietnam using beachrock and beach-ridge deposits. Glob. Planet. Change 110, 214–222.

Tamura, T., 2012. Beach ridges and prograded beach deposits as palaeoenvironment records. Earth-Sci. Rev. 114, 279–297. https://doi.org/10.1016/j.earscirev.2012.06.004

Tamura, T., Nanayama, F., Saito, Y., Murakami, F., Nakashima, R., Watanabe, K., 2007. Intra-shoreface erosion in response to rapid sea-level fall: depositional record of a tectonically uplifted strand plain, Pacific coast of Japan. Sedimentology 54, 1149–1162.

Taylor, M., Stone, G.W., 1996. Beach-Ridges: A Review. J. Coast. Res. 12.

US Geological Survey, 2022. 1-meter Digital Elevation Model.

US Geological Survey, 2011. National Elevation Dataset, 1/9 arc-second.

Wolff, E.W., Mulvaney, R., Grieman, M.M., Hoffmann, H.M., Humby, J., Nehrbass-Ahles, C., Rhodes, R.H., Rowell, I.F., Sime, L.C., Fischer, H., Stocker, T.F., Landais, A., Parrenin, F., Steig, E.J., Dütsch, M., Golledge, N.R., 2025. The Ronne Ice Shelf survived the last interglacial. Nature 638, 133–137. https://doi.org/10.1038/s41586-024-08394-w

Yau, A.M., Bender, M.L., Robinson, A., Brook, E.J., 2016. Reconstructing the last interglacial at Summit, Greenland: Insights from GISP2. Proc. Natl. Acad. Sci. 113, 9710–9715. https://doi.org/10.1073/pnas.1524766113

Zhou, Y., McManus, J., 2022. Extensive evidence for a last interglacial Laurentide outburst (LILO) event. Geology 50, 934–938. https://doi.org/10.1130/G49956.1

Zurbuchen, J., Simms, A.R., Warrick, J.A., Miller, I.M., Ritchie, A., 2020. A model for the growth and development of wave-dominated deltas fed by small mountainous rivers: Insights from the Elwha River delta, Washington. Sedimentology 67, 2310–2331.